HAL
open science

A Novel Approach for Ridge Detection and Mode Retrieval of Multicomponent Signals Based on STFT

Nils Laurent, Sylvain Meignen

To cite this version:

Nils Laurent, Sylvain Meignen. A Novel Approach for Ridge Detection and Mode Retrieval of Multicomponent Signals Based on STFT. 2020. hal-02945707v1

HAL Id: hal-02945707

https://hal.science/hal-02945707v1

Preprint submitted on 25 Sep 2020 (v1), last revised 1 Apr 2022 (v2)

HAL is a multi-disciplinary open access archive for the deposit and dissemination of scientific research documents, whether they are published or not. The documents may come from teaching and research institutions in France or abroad, or from public or private research centers.

L'archive ouverte pluridisciplinaire **HAL**, est destinée au dépôt et à la diffusion de documents scientifiques de niveau recherche, publiés ou non, émanant des établissements d'enseignement et de recherche français ou étrangers, des laboratoires publics ou privés.

A Novel Approach for Ridge Detection and Mode Retrieval of Multicomponent Signals Based on STFT

Nils Laurent, Sylvain Meignen

Abstract

Time-frequency analysis is often used to study non stationary multicomponent signals, which can be viewed as the surperimposition of modes, associated with ridges in the TF plane. To understand such signals, it is essential to identify their constituent modes. This is often done by performing ridge detection in the time-frequency plane which is then followed by mode retrieval. Unfortunately, existing ridge detectors are often not enough robust to noise therefore hampering mode retrieval. In this paper, we therefore develop a novel approach to ridge detection and mode retrieval based on the analysis of the short-time Fourier transform of multicomponent signals in the presence of noise, which will prove to be much more robust than state-of-the-art methods based on the same time-frequency representation.

Index Terms

AM/FM multicomponent signals, Short-time Fourier transform, Ridge detection, Mode retrieval.

I. Introduction

Many signals such as audio signals (music, speech, bird songs) [1], medical data (electrocardiogram, thoracic and abdominal movement signals), can be modeled as a superimposition of amplitude- and frequency-modulated (AM-FM) modes [2], [3], and are therefore called *multicomponent signals* (MCSs). Time-frequency analysis is often used to deal with such signals [4]–[6], since their modes are associated with curves in the *time-frequency* (TF) plane, called *ridges*. To extract these ridges is essential when one is interested in separating a MCS into its constituent modes [7]. For that purpose, several TF-based techniques were developed [8] [9] using the idea that the ridges correspond to local maxima along the frequency axis of the modulus of some *time-frequency representation* (TFR). Indeed, it was shown in [10], [11] that these maxima approximate the *instantaneous frequency* (IF) of the modes, the quality of approximation depending on the noise level and on the length of the analysis window. This concept has

then been used on various types of TFRs such as for instance the *short-time Fourier transform* (STFT) [12], [13], or *synchrosqueezed transforms* either based on the continuous wavelet transform [14] or STFT [15]–[17]. TF ridges are also used in demodulation approaches still developed for the purpose of *mode retrieval* (MR) [18], [19]. An alternative TF-based MR technique, not explicitly using ridge detection, consists of finding locally the linear chirp that fits the best the STFT of the signal [20].

The main limitation of the above techniques is that at high noise level, the local maxima along the frequency axis that define the ridges in the noiseless case may no longer exist. In this regard, the analysis of these maxima proposed in [10] assumes a low noise level. In case of high noise level, a study was carried out on the TFR associated with the *Wigner-Ville distribution* (WVD) in [21], basically remarking that peak searching based techniques are not able to cope with multicomponent or monocomponent signals contaminated by strong noise. The key ideas of the algorithm proposed in [21] were first that, if the WVD maximum at the considered time instant is not at the IF point, there is a high probability that the IF is at a point having one of the largest WVD values. The second argument was based on the assumption that the IF variations between two consecutive points is not extremely large.

Following [21], it seems to be possible to follow the ridges by considering local maxima and then by chaining them using some proximity criterion in the TF plane. However, as we will see, when one considers STFT as TFR, the noise can generate zeros in the vicinity of true IF location splitting the ridge into two chains of local maxima. It is therefore illusory to try and build the ridges by simply chaining local maxima in the TF plane. The second argument used in [21] is however very interesting in that even, at a high noise level, the local maxima associated with the signal components are close in the TF plane.

Though there exist many different techniques to extract the ridges in the TF plane, mainly using optimization procedures as in [9], [22], they rely on an initial so-called *skeleton of the transform* which is usually not available in heavy noise situations. Indeed, to reconstruct the modes, these approaches use modified versions of *least-square minimizations* in which the data terms are ridge points, supposed to be reliable enough otherwise the algorithms fail. However, to assign a TF point to a specific ridge is probably one of the most complicated aspect of RD and should be handled with care. To perform this kind of initial estimation of ridge points, one needs to carefully analyze the behavior of the coefficients of the TFR in the vicinity of local maxima. In the present paper, to accurately assign a TF point to a ridge, we will make the assumption that the modes are not crossing, our goal being to improve RD in the TF plane in very noisy situations in a fully adaptive way. It is however possible to deal with crossing modes by imposing regularity constraints on the extracted modes in the TF plane [8], [9], [15], or by analyzing the signal in the time domain using a parametric approach [23], but this is not the scope of the present paper.

Indeed, we aim to propose a fully adaptive RD that is very competitive in noisy situations. For that purpose, we will first analyze carefully the energy in the TF plane in the vicinity of local maxima. In particular, we will see that some of these local maxima can be gathered into so-called *relevant ridge portions* (RRPs) that will be the basis to our new approach. As already mentioned in the context of WVD [21], the effect of noise on TF ridges is to split them into ridge portions that need to be identified and then gathered together when they correspond to the same mode. This is in essence the goal we pursue in the present paper. The paper is organized as follows: in Section II, we recall basic notations regarding STFT and MCSs as well the most commonly used TF-based RD technique. Since the latter depends on several arbitrary parameters, we recall in Section III, how it can be made more adaptive by using a local chirp rate estimate, as recently proposed in [13]. Then, taking into account that, in noisy situations, a mode cannot be associated with a single ridge computed from chaining local maxima in the TF plane, we alternatively consider that it corresponds to a set of so-called *relevant ridge portions* (RRPs), which are defined in Section IV. This helps us define a new RD technique in Section V. Section VI is then devoted to the comparison of the proposed new technique to state-of-the-art TF-based methods for RD and MR, highlighting the improvement brought by the former especially in the presence of heavy noise. An application to the analysis of gravitational-wave concludes the paper.

II. Definitions and Notations

A. Short-Time Fourier Transform

Let $\tilde{f}$ be a discrete signal of length L altered by an additive noise ε, and such that $\tilde{f}[n] = \tilde{f}(\frac{n}{L})$:

$$\tilde{f} := f + \varepsilon, \tag{1}$$

and g a discrete real window supported on $[-\frac{M}{L}, \frac{M}{L}]$. In that context, we define the *short time Fourier transform* (STFT) as follows:

$$V_{\tilde{f}}^{g}[m,k] := \sum_{n=0}^{N-1} \tilde{f}[n+m-M]g[n-M]e^{-2i\pi\frac{k}{N}(n-M)}, \tag{2}$$

with $2M+1 \leq N$, where N is the number of frequency bins, the index k corresponding to the frequency $k\frac{L}{N}$. The STFT of the signal $\tilde{f}$ is invertible, provided $g[0] \neq 0$, since one has:

$$\tilde{f}[n] = \frac{1}{g[0]N} \sum_{k=0}^{N-1} V_{\tilde{f}}^{g}[n,k]. \tag{3}$$

B. Multicomponent Signal Definition

In this paper, we will intensively study MCSs defined as a superimposition of AM-FM components or modes:

$$f[n] = \sum_{p=1}^{P} f_p[n] \quad \text{with} \quad f_p[n] = A_p[n] e^{i2\pi\phi_p[n]}, \tag{4}$$

for some finite $P \in \mathbb{N}$, $A_p[n]$ and $\phi_p'[n]$ being respectively the instantaneous amplitude (IA) and frequency (IF) of f_p satisfying: $A_p[n] > 0, \phi_p'[n] > 0$ and $\phi_{p+1}'[n] > \phi_p'[n]$ for each time index n.

We also assume that A_p is differentiable with $|A_p'[n]|$ small compared with $\phi_p'[n]$, that the modes are separated with resolution Δ and their modulations are bounded by B_f, i.e. for each time index n,

$$\begin{aligned} \forall\ 1 \leq p \leq P-1,\ \phi_{p+1}'[n] - \phi_p'[n] > 2\Delta \\ \forall\ 1 \leq p \leq P,\ |\phi_p''[n]| \leq B_f. \end{aligned} \tag{5}$$

C. Classical Ridge Detection

A commonly used RD approach was originally proposed in [8], and then used in [14]. The goal is to compute an integer estimate $\varphi_p[n]$ of $\phi_p'[n]N/L$ by extracting, on the spectrogram, a ridge corresponding to mode p. This is actually done by computing

$$\max_{\boldsymbol{\varphi}} \sum_{\substack{1 \leq p \leq P \\ 0 \leq n \leq L-1}} |V_f^g[n, \varphi_p[n]]|^2 - \alpha\left(\frac{\Delta^1 \varphi_p[n] L^2}{N}\right)^2 - \beta\left(\frac{\Delta^2 \varphi_p[n] L^3}{N}\right)^2, \tag{6}$$

with $\boldsymbol{\varphi} = (\varphi_p)_{p=1,\cdots,P}$ where $\varphi_p : \{0, \cdots, L-1\} \mapsto \{0, \cdots, N-1\}$, α and β both positive, and in which $\frac{\Delta^1 \varphi_p[n] L^2}{N} = \frac{(\varphi_p[n+1] - \varphi_p[n]) L^2}{N}$ and $\frac{\Delta^2 \varphi_p[n] L^3}{N} = \frac{(\varphi_p[n+1] - 2\varphi_p[n] + \varphi_p[n-1]) L^3}{N}$, are approximations of $\phi_p''[n]$ and $\phi_p'''[n]$.

Taking into account that regularization terms associated with α and β are not relevant when a ridge is associated with a local maximum of the STFT magnitude and that to consider such penalization parameters in noisy situations leads to inaccurate IF estimation [19], one can alternatively put a bound on the frequency modulation allowed while extracting the ridges, and then replace (6) by a *peeling algorithm* where a first mode is extracted as follows [13]:

$$\max_{\varphi_1} \sum_{n=0}^{L-1} |V_f^g[n, \varphi_1[n]]|^2, \quad \text{s.t. } |\Delta^1 \varphi_1[n]| \frac{L^2}{N} \leq B_f. \tag{7}$$

Then, after φ_1 is computed, one defines $V_{f,0}^g := V_f^g$, and RD continues replacing $V_{f,0}^g$ by:

$$V_{f,1}^g[n,k] := \begin{cases} 0, \text{ if } \varphi_1[n] - \lceil \frac{\Delta N}{L} \rceil \leq k \leq \varphi_1[n] + \lceil \frac{\Delta N}{L} \rceil \\ V_{f,0}^g[n,k], \text{ otherwise,} \end{cases} \tag{8}$$

in which $\lceil X \rceil$ is the smallest integer larger than X. This then enables the computation of φ_2 replacing V_f^g by $V_{f,1}^g$ in (7), and then the definition of $V_{f,2}^g$ from $V_{f,1}^g$ the same way as $V_{f,1}^g$ from $V_{f,0}^g$. Such a procedure is iterated until P ridges $(\varphi_p)_{p=1,\cdots,P}$ are extracted.

In practice, to compute a candidate for φ_1, one first fixes an initial time index n_0, computes

$$k_0 := \underset{0 \leq k \leq N-1}{\text{argmax}} \, |V_f^g[n_0, k]|, \tag{9}$$

and puts $\varphi_1[n_0] := k_0$. Then, to define φ_1 on $\{n_0 + 1, \cdots, L-1\}$, one uses the following recurring principle starting from $n = n_0$:

$$\varphi_1[n+1] := \underset{k}{\text{argmax}} \left\{ |V_f^g[n+1, k]|, \varphi_1[n] - \lceil \frac{NB_f}{L^2} \rceil \leq k \leq \varphi_1[n] + \lceil \frac{NB_f}{L^2} \rceil \right\}. \tag{10}$$

The same principle is applied on $\{0, \cdots, n_0 - 1\}$, again starting from $n = n_0$ but replacing $n+1$ by $n-1$ in (10). Finally, other initialization time indices than n_0 are considered to define other candidates for φ_1, the ridge finally kept being the one among all candidates, maximizing the energy in the TF plane, i.e. $\sum_n |V_f^g[n, \varphi_1[n]]|^2$. This RD will be called *Simple Ridge Detection* (S-RD) in the sequel.

There are however two strong limitations to S-RD. The first one is that, in a noisy context, each mode cannot be associated at each time instant with a local maximum of $|V_{\tilde{f}}^g|$ along the frequency axis. As a result, S-RD enforces the extraction of P ridges even when these are not associated with modes. This is illustrated in Fig. 1, in which we first display, in Fig. 1 (a), the magnitude of the STFT of a linear chirp along with the three largest local maximum along the frequency axis at each time instant: we see that these maxima are not chained in the TF plane. To have a clearer view of the effect of noise on the ridge we display in Fig. 1 (b), a zoom on a region containing the expected ridge location and corresponding to the situation where a global maximum along the frequency axis is split into two local maxima. In such a case, it transpires that the noise generates a zero of the STFT close to the location of the IFs of the modes, surrounded by two local maxima. This is the reason why any technique defining the ridge by following the local maxima along the frequency axis will result in poor IF estimation. Such a paradigm is however the basis to RD technique like S-RD, and one of the goal of the present paper is to circumvent this limitation. Note that this figure also illustrates the dependency of RD techniques such as S-RD on the initialization time n_0. The second important drawback of S-RD is that the upper bound B_f for the modulation is fixed a priori: S-RD does not take into account the value of the modulation and even not its sign. To deal with this issue is also one of the aim of the present paper. In this regard, we first recall in the following section how to introduce some kind of adaptivity in RD by removing the dependence of S-RD on upper frequency bound B_f, as proposed in [13].

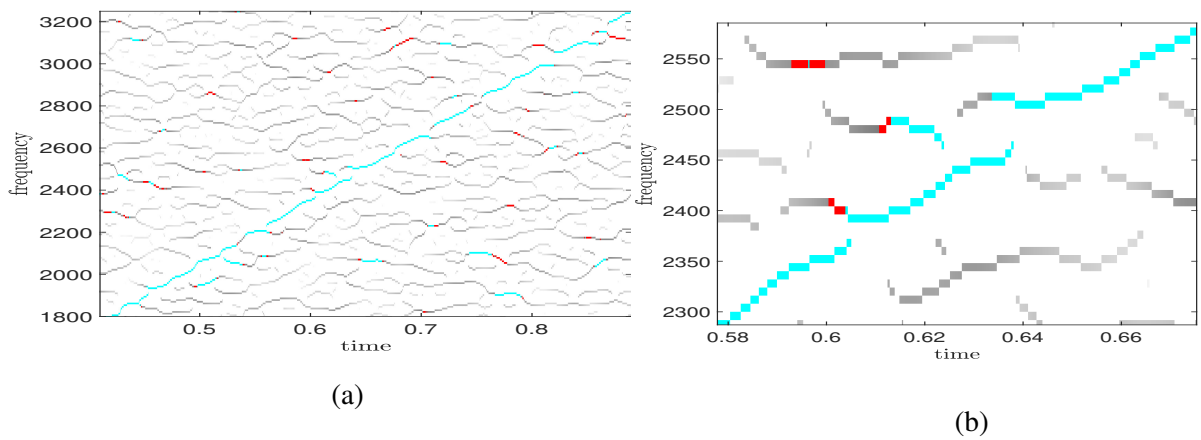

Fig. 1. (a): Magnitude of the STFT of a noisy linear chirp along with its maxima along the frequency axis; (b): Zoom on the effect of noise on local maxima; Cyan coefficients are among the two largest coefficients along the frequency axis, red ones correspond to the third largest along the frequency axis.

III. Fully Adaptive Ridge Detection

To circumvent the lack of adaptivity in S-RD, a novel approach called *modulation based ridge detection* (MB-RD) was proposed in [13]. In a nutshell, this approach considers the complex approximation of the modulation of the mode used in the definition of the *second order synchrosqueezing transform* and defined as [17]:

$$\tilde{q}_f[n,k] = \frac{1}{2i\pi}\frac{V_f^{g''}[n,k]V_f^{g}[n,k] - (V_f^{g'}[n,k])^2}{V_f^{tg}[n,k]V_f^{g'}[n,k] - V_f^{tg'}[n,k]V_f^{g}[n,k]}, \tag{11}$$

in which $V_f^{g'}, V_f^{tg}, V_f^{g''}, V_f^{tg'}$ are respectively STFTs of f computed with windows $n \mapsto g'[n], (tg)[n], g''[n]$ and $(tg')[n]$. In that context, $\hat{q}_f[n,k] = \Re\{\tilde{q}_f[n,k]\}$ consists of an estimate of the modulation of the closest mode to $[n,k]$ in the TF plane. To extract the first ridge MB-RD uses the same recurring principle as S-RD introduced in Section II-C, but, instead of defining φ_1 with B_f as upper bound for the modulation, MB-RD uses $\hat{q}_f$ and a constant $C > 0$, meaning (10) is replaced by:

$$\varphi_1[n+1] := \underset{k}{\operatorname{argmax}} \left\{ |V_f^g[n+1,k]|, \varphi_1[n] + \lceil \hat{q}_f[n,\varphi_1[n]]\frac{N}{L^2} \rfloor - C \leq k \leq \varphi_1[n] + \lceil \hat{q}_f[n,\varphi_1[n]]\frac{N}{L^2} \rfloor + C \right\}, \tag{12}$$

in which $\lceil X \rfloor$ is the closest integer to X, the user-defined constant C compensating for potential estimation errors. The motivation for (12) lies in the fact that $\hat{q}_f$ is a first order estimate of ϕ_1'' corresponding to the local orientation of the ridge.

Though MB-RD improves S-RD in that it is more adaptive, both techniques are based on the assumption that a mode generates a significant local maximum along the frequency axis at each time instant, which

is not the case in heavy noise situations. Another limitation is that since the ridges are extracted one after the other using a *peeling algorithm* [13], if RD fails for one mode then the detection process will also most probably fail for the next ones. To deal with this issue, we propose, in the following section, to introduce the concept of *relevant ridge portions* (RRPs) that will be subsequently used to define our new RD technique. It will consist in computing all the ridges simultaneously, thus getting rid of the traditional peeling algorithm.

IV. Definition of Relevant Ridge Portions

Let us consider, for the sake of simplicity that g is the Gaussian window $g[n] = e^{-\pi \frac{n^2}{\sigma^2 L^2}}$, for which it can be shown that if f is a linear chirp with constant amplitude A, i.e. $f[n] = Ae^{2i\pi\phi[n]}$ with ϕ'' a constant function, one has [17]:

$$|V_f^g[n,k]| \approx AL\sigma(1+\sigma^4\phi''[n]^2)^{-\frac{1}{4}} e^{-\pi \frac{\sigma^2(k\frac{L}{N}-\phi'[n])^2}{1+\sigma^4\phi''[n]^2}}, \tag{13}$$

whose standard deviation is:

$$\frac{1}{\sqrt{2\pi}\sigma}\sqrt{1+\sigma^4\phi''[n]^2} \approx std_{LC}[n,\varphi[n]] := \frac{1}{\sqrt{2\pi}\sigma}\sqrt{1+\sigma^4\hat{q}_f[n,\varphi[n]]^2}. \tag{14}$$

We then define an interval corresponding to this standard deviation around $\varphi[n]$, the global maximum of $|V_f^g|$ along the frequency axis at time index n, namely:

$$I_{LC}[n,\varphi[n]] = \left[\lfloor \varphi[n] - std_{LC}[n,\varphi[n]]\frac{N}{L}\rfloor, \lceil \varphi[n] + std_{LC}[n,\varphi[n]]\frac{N}{L}\rceil\right]. \tag{15}$$

For a MCS defined as in (4), at each time instant n, $|V_f^g|$ admits P local maxima along the frequency axis, and for each of them, one can define an interval I_{LC} by considering that each mode can be locally approximated by a linear chirp. Now, if some noise is added to f to obtain $\tilde{f}$, some other local maxima not associated with a mode arise in the TF plane. As the magnitude of $|V_{\tilde{f}}^g|$ at a local maximum is usually larger when it corresponds to a mode rather than to noise, we strengthen these maxima by first computing at each local maximum $[n,k_0]$, the interval $I_{LC}[n,k_0]$, and then by defining the auxiliary variable:

$$S_{LC}[n,k_0] = \sum_{k\in I_{LC}[n,k_0]} |V_{\tilde{f}}^g[n,k]|^2. \tag{16}$$

Using the variable S_{LC}, we then construct P ridge portions starting at time index n_0, by considering $(\varphi_p[n_0])_{p=1,\cdots,P}$ such that $(S_{LC}[n_0,\varphi_p[n_0]])_{p=1,\cdots,P}$ are the P largest local maxima at time index n_0. From each of these points, we define ridge portions using a variant of (12), by introducing first $\psi_p[n_0+1] := \varphi_p[n_0] + \lceil \hat{q}_{\tilde{f}}[n_0,\varphi_p[n_0]]\frac{N}{L^2}\rfloor$, and then

$$\varphi_p[n_0+1] := \underset{k}{\operatorname{argmin}}\left\{|k-\psi_p[n_0+1]|,\ \text{s.t. } S_{LC}[n_0+1,k] \text{ is a local maximum}\right\}. \tag{17}$$

The differences with (12) is that we use S_{LC} instead of $V_{\tilde{f}}^{g}$ and that, for mode p, we look for the closest maximum to $\psi_p[n_0+1]$ along the frequency axis of S_{LC}, thus avoiding the use of an extra parameter C. Then $[n_0+1, \varphi_p[n_0+1]]$ belongs to the ridge starting at $[n_0, \varphi_p[n_0]]$ only if $S_{LC}[n_0+1, \varphi_p[n_0+1]]$ is among the $2P+1$ largest maxima of S_{LC} at time index n_0+1, otherwise the ridge construction is stopped. To consider the $2P+1$ largest maxima is motivated by the fact that when a local maximum corresponding to a ridge is destroyed by the noise it often gives rise to two maxima as illustrated in Fig. 1 (b), therefore the $2P$. largest maxima not to miss any information. Then, we add one to take into account the fact that locally some maxima related to noise may be larger than some others related to signal.

The procedure is then iterated forward and backward (from n_0) until the construction of each of the P ridge portions is stopped. Thus, with such a formulation, each initialization point n_0 leads to P ridge portions, with a priori different lengths. It is important to mention that, contrary to MB-RD and S-RD, we do not construct the ridges one by one using a so-called *peeling algorithm* as in [13], [14], [17], [20], but alternatively construct P ridge portions at a time, and do not impose that the ridge portions starting at time n_0 last for the whole time span.

Now, investigating the stability of these ridge portions with respect to the initialization point n_0, we consider other initialization points around n_0, and compute the associated P ridge portions using the just described procedure. If a ridge portion computed at time index n_0 is present in the set of the P ridge portions for s successive initialization time indices including n_0, the latter consists of a *relevant ridge portion* (RRP) at scale s.

V. RD Based on RRPs

In this section, we are going to build a new RD technique based on RRPs. For that purpose, we first introduce a procedure to gather the RRPs associated with the same mode, and then explain how to build RD from these gathered RRPs.

A. Gathering RRPs Based on TF Location

Our motivation to gather RRPs is that though heavy noise splits the ridge associated with a mode in many different RRPs, these remain close to each other in the TF plane, following [21] in that matter. Our goal is thus to associate to a mode a set of RRPs by defining the notion of *intersection* for $RRPs$. For that purpose, let us denote $(\mathcal{R}_j)_{j\in J}$ the set of RRPs. For each $\mathcal{R}_i$, we denote $[n_0, k_0]$ and $[n_1, k_1]$

the beginning and the end of $\mathcal{R}_i$, then define $I_{PH}[k] = \left[\lfloor k - \frac{3N}{L\sqrt{2\pi}\sigma}\rfloor, \lceil k + \frac{3N}{L\sqrt{2\pi}\sigma}\rceil\right]$ (PH standing for *pure harmonic*). Using these notations, we define the neighborhood of $\mathcal{R}_i$, as follows:

$$\begin{aligned}\mathcal{N}\mathcal{R}_i = \{[n,l], n \in [n_0 - \Delta t, n_0], l \in I_{PH}[k_0]\} \bigcup \{[n,l], [n,k] \in \mathcal{R}_i \text{ and } l \in I_{PH}[k]\} \\ \bigcup \{[n,l], n \in [n_1, n_1 + \Delta t], l \in I_{PH}[k_1]\}\,.\end{aligned} \tag{18}$$

At each location on a RRP, the frequency neighborhood consists of the interval corresponding to 3 times the standard deviation computed assuming no modulation (because to take into account the modulation in that context may lead to instabilities), and at each end of an RRP we extend this neighborhood using the time parameter Δt, which corresponds to the maximal time distance, measured in number of time bins, between successive RRPs associated with the same mode.

In that context, we say that $\mathcal{R}_i$ and $\mathcal{R}_j$ are intersecting if $\mathcal{N}\mathcal{R}_i \bigcap \mathcal{N}\mathcal{R}_j \neq \emptyset$. All the intersecting RRPs are then gathered together to obtain a set $(\mathcal{M}_q)_{q\in Q}$, that is each $\mathcal{M}_q$ is the union of some RRPs, and we then define the energy of $\mathcal{M}_q$ as:

$$R(\mathcal{M}_q) = \sum_{[m,l]\in\mathcal{M}_q} S_{LC}[m,l]. \tag{19}$$

All the points in $\mathcal{M}_q$ are then given the energy $R(\mathcal{M}_q)$. Finally, we only keep in $\mathcal{M}_q$ only one TF point per time index: if there are several TF points in $\mathcal{M}_q$ associated with one time index we only keep in $\mathcal{M}_q$ the one associated with the most energetic RRP (the energy of $\mathcal{R}_i$ being defined as $R(\mathcal{R}_i)$).

B. Definition of New RD Technique

For the sake of simplicity let us now assume that the set $\mathcal{M} = (\mathcal{M}_q)_{q\in Q}$ is ranked according to decreasing energies. Starting from $q = 0$, we consider the first index q_0 such that P elements in $(\mathcal{M}_q)_{q=0,\cdots,q_0}$ contains some points associated with the same time index. Let us denote $(\mathcal{M}_p^0)_{p=1,\cdots,P}$, the corresponding elements of $\mathcal{M}$, ranked according to increasing frequencies. To obtain a first approximation of the pth ridge, we compute the following polynomial approximation:

$$D_p^0 = \underset{D}{\text{argmin}} \sum_{[n,k]\in\mathcal{M}_p^0} |k - D(\frac{n}{L})|^2 R(\mathcal{M}_p^0)^2,\ p = 1, \cdots, P, \tag{20}$$

where D is some polynomial of degree d. We then associate with each polynomial D_p^0 a TF region defined as:

$$\mathcal{TF}_{D_p^0} = \left\{[n,k],\ 0 \leq n \leq L-1,\ k \in I_{PH}(D_p^0(\frac{n}{L})),\right\} \tag{21}$$

in which $I_{PH}(D_p^0(\frac{n}{L}))$ corresponds to the definition given in the previous section except we use round brackets instead of square brackets since $D_p^0(\frac{n}{L})$ is not located on the frequency grid.

If the TF regions $(\mathcal{TF}_{D_p^0})_{p=1,\cdots,P}$ intersect some elements in $\mathcal{M}$ other than $(\mathcal{M}_p^0)_{p=1,\cdots,P}$ then the corresponding RRPs are added, with the corresponding energy, in minimization (20), and updated approximation polynomials are computed. Such a procedure is iterated until no new elements in $\mathcal{M}$ are intersected by the updated $(\mathcal{TF}_{D_p^0})_{p=1,\cdots,P}$ (for the sake of simplicity, we still denote by $(D_p^0)_{p=1,\cdots,P}$ the set of polynomials obtained after these iterations). Finally, we define the energy corresponding to these polynomial approximations as follows:

$$E^0 := \sum_{p=1}^{P}\sum_{n=0}^{L-1} S_{LC}(n, D^0_(\frac{n}{L})), \tag{22}$$

in which the round brackets are used to mean $D_p^0(\frac{n}{L})$ is not necessarily on the frequency grid. The set $(D_p^0)_{p=1,\cdots,P}$ consists of a first approximation for the P ridges. Then, we consider the next index q_1 larger than q_0 such that there exists a subset $(\mathcal{M}_p^1)_{p=1,\cdots,P}$ of $(\mathcal{M}_q)_{q=0,\cdots,q_1}$ having one time index in common and different from $(\mathcal{M}_p^0)_{p=1,\cdots,P}$. Solving the updated optimization problem for each p:

$$D_p^1 = \underset{D}{\operatorname{argmin}} \left(R(\mathcal{M}_p^0)\right)^2 \sum_{[n,k]\in\mathcal{M}_p^0} |k - D(\frac{n}{L})|^2 + \left(R(\mathcal{M}_p^1)\right)^2 \sum_{[n,k]\in\mathcal{M}_p^1} |k - D(\frac{n}{L})|^2, \tag{23}$$

and then iterating as explained before, we get an updated set of approximation polynomials which we call $(D_p^1)_{p=1,\cdots,P}$, to which we associate the energy E^1 following (22). If $E^1 > E^0$, then the approximation polynomials become the set $(D_p^1)_{p=1,\cdots,P}$, otherwise one keeps the original set $(D_p^0)_{p=1,\cdots,P}$. Such a procedure is iterated until all the elements in $\mathcal{M}$ have been considered, and we end up with a set of polynomials called $(D_p^{fin})_{p=1,\cdots,P}$. We finally rerun this procedure starting with $(D_p^{fin})_{p=1,\cdots,P}$ as initial polynomials values and replacing $I_{PH}(D^0(\frac{n}{L}))$ by $\tilde{I}_{LC}(n, D_p^{fin}(\frac{n}{L}))$, defined by:

$$\tilde{I}_{LC}(n, D_p^{fin}(\frac{n}{L})) = \left[\lfloor D_p^{fin}(\frac{n}{L})) - 3std_{LC}(n, D_p^{fin}(\frac{n}{L}))\frac{N}{L}\rfloor, \lceil D_p^{fin}(\frac{n}{L})) + 3std_{LC}(n, D_p^{fin}(\frac{n}{L}))\frac{N}{L}\rceil\right], \tag{24}$$

with $std_{LC}(n, D_p^{fin}(\frac{n}{L})) := \frac{1}{\sqrt{2\pi}\sigma}\sqrt{1+\sigma^4(D_p^{fin})'(\frac{n}{L})^2}$. This post-processing step enables to take into account some ridge portions that were wrongly left apart. Note that if the final set of polynomials obtained at the end the procedure is such that the polynomials are intersecting, we consider instead the set of non intersecting polynomials obtained with the just described procedure and associated with the largest energy. For the sake of simplicity, we still denote by $(D_p^{fin})_{p=1,\cdots,P}$ this final set of approximation polynomials.

In the sequel, we denote $[F_p^-[n], F_p^+[n]] := \tilde{I}_{LC}(n, D_p^{fin}(\frac{n}{L}))$, and we omit p in the case of a monocomponent signal. Furthermore, the set of RRPs used in the construction of $(D_p^{fin})_{p=1,\cdots,P}$ are denoted by $(\mathcal{M}_p^{fin})_{p=1,\cdots,P}$. From now on, the proposed RD method is called RRP-RD. Note that for particular applications, in particular when the phases of the modes contain fast oscillations, polynomial approximation may be replaced by spline approximation, as illustrated in Section VI-C on a gravitational wave signal.

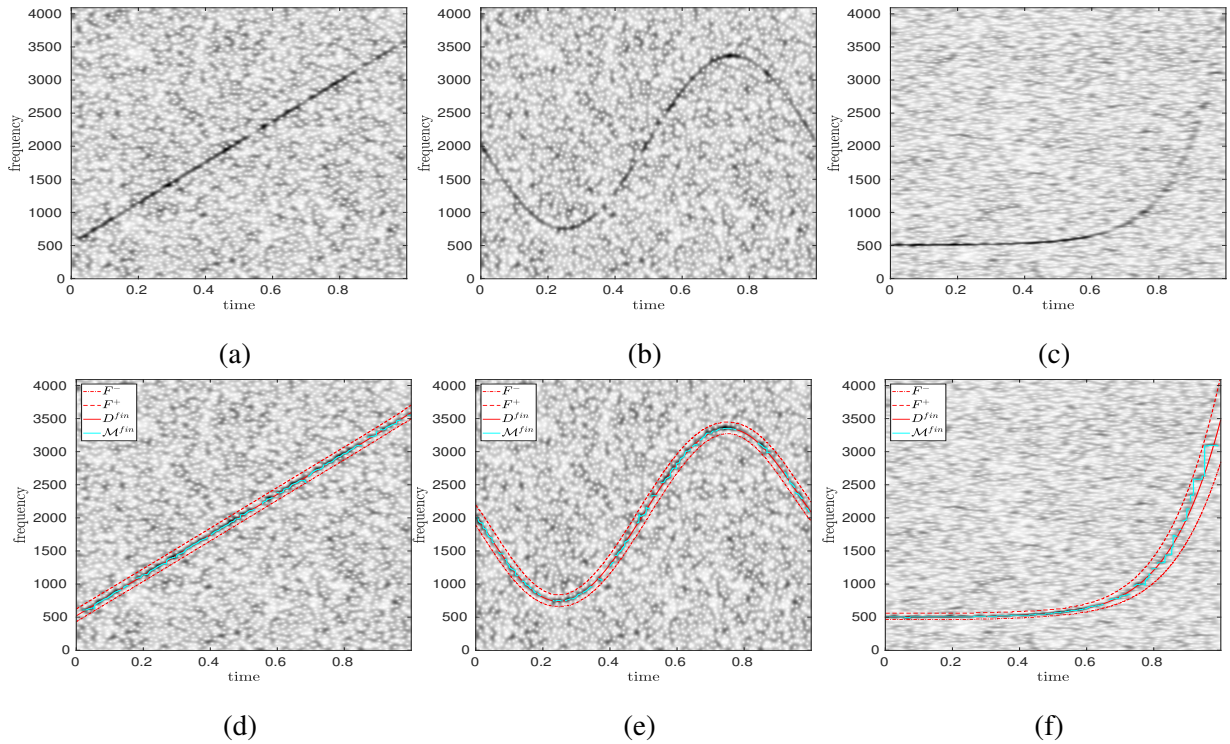

Fig. 2. (a): STFT of a noisy linear chirp (SNR = -10 dB); (b): STFT of a noisy mode with cosine phase (SNR = -10 dB); (c): STFT of a noisy mode with exponential phase (SNR = -10 dB); (d): ridge D^{fin} detected for the signal displayed in (a), with the set of RRPs $\mathcal{M}^{fin}$ used in the computation of the ridge D^{fin}, along with $F^-[n]$ and $F^+[n]$ for each n; (e): same as (d) but for the signal whose STFT is displayed in (b); (f): same as (d) but for the signal whose STFT is displayed in (c)

We display in Fig. 2 an illustration of the proposed RD on a noisy linear chirp, a noisy mode with cosine phase, and a noisy mode with exponential phase (displayed on the first row of that figure). In each case, the noise is a complex Gaussian noise and the noise level corresponds to an input SNR of -10 dB (the input SNR is defined as $SNR(f,\tilde{f}) = 20\log_{10}\left(\frac{\|f\|_2}{\|\tilde{f}-f\|_2}\right)$). On the second row of Fig. 2, we display D^{fin} along with the RRPs used for its construction, namely $\mathcal{M}^{fin}$, and also the interval $[F^-[n], F^+[n]]$ for each n. These first illustrations show that the proposed procedure seems to be efficient in very noisy situations ; this will be further quantified in Section VI. We also illustrate the procedure on the two mode signals of Fig. 3, which consist either of two linear chirps, two modes with cosine phase, and a last signal made of a linear chirp plus an exponential chirp. The input SNR is still fixed to -10 dB. We again notice that RRP-RD seems to be well adapted to deal with MCS in the presence of heavy noise, regardless of the modulation of the modes.

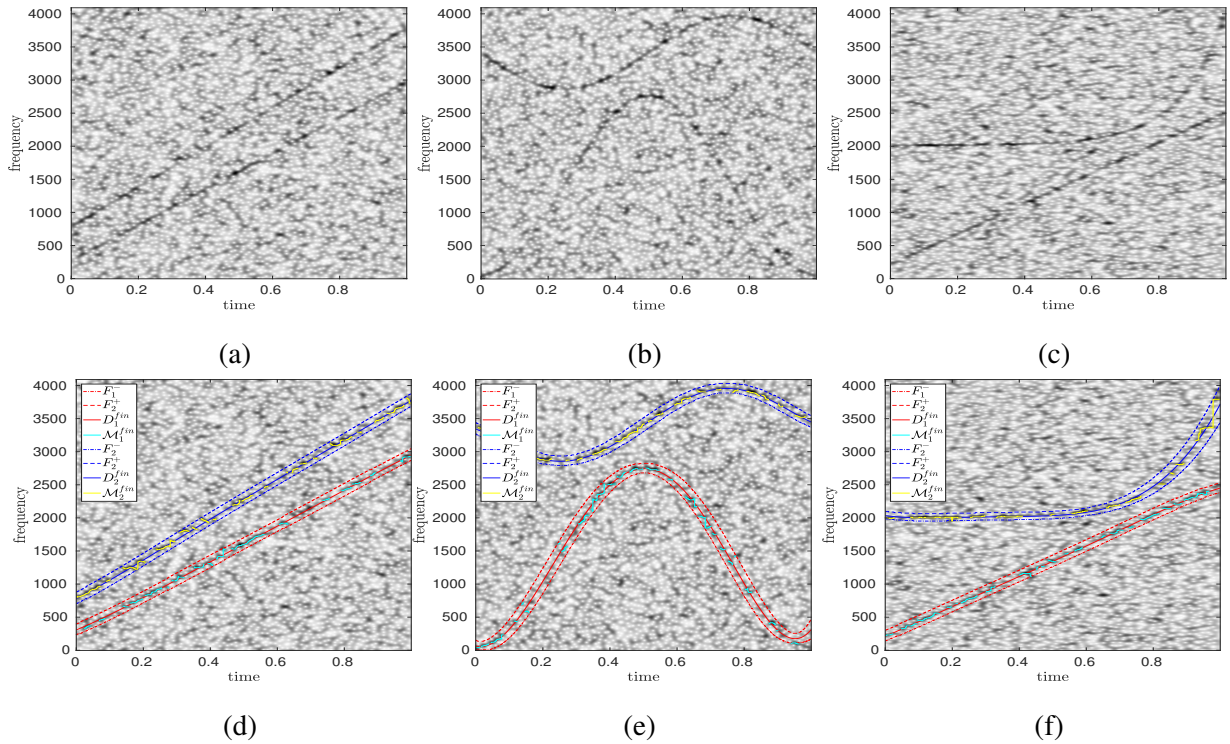

Fig. 3. (a): STFT of two noisy linear chirps (SNR = -10 dB); (b): STFT of two noisy modes with cosine phases, with different modulation (SNR = -10 dB); (c): STFT of a signal made of a linear chirp and a mode with exponential phase (SNR = -10 dB); (d): ridges $(D_p^{fin})_{p=1,2}$ detected for the signal displayed in (a), along with $(\mathcal{M}_p^{fin})_{p=1,2}$. We also display the interval $[F_p^-[n], F_p^+[n]]$, for each n and p; (e): same as (d) but for the signal whose STFT is displayed in (b); (f): same as (d) but for the signal whose STFT is displayed in (c).

C. Mode Reconstruction

Having defined RRP-RD, we explain how we proceed with mode reconstruction. A simple strategy consists of summing the coefficients in $[F_p^-[n], F_p^+[n]]$ for each n, namely

$$f_p[n] \approx \frac{1}{g[0]N} \sum_{k \in [F_p^-[n], F_p^-[n]]} V_{\tilde{f}}^g[n,k]. \tag{25}$$

To take into account the fact that the intervals $[F_p^-[n], F_p^+[n]]$ and $[F_{p+1}^-[n], F_{p+1}^+[n]]$ may intersect for some time index, in such instances these intervals are replaced by $[F_p^-[n], \frac{F_p^+[n]+F_{p+1}^-[n]}{2}]$ and $[\frac{F_p^+[n]+F_{p+1}^-[n]}{2}, F_{p+1}^+[n]]$ respectively. This reconstruction procedure is denoted by RRP-MR in the sequel.

An alternative technique for mode reconstruction was recently proposed in [24], and is based on a linear chirp approximation for the mode. In our context, the technique proposed in [24] would consider $k_0 := \lfloor D_p^{fin}[n]\frac{N}{L} \rceil$, and then the following approximation for the STFT of f_p (see [24] for details):

$$V_{f_p}^g[n,k] \approx V_{\tilde{f}}^g[n,k_0] e^{\frac{\pi\sigma^2(1+i(D_p^{fin})'(\frac{n}{L})\sigma^2)}{1+(D_p^{fin})'(\frac{n}{L})^2\sigma^4}\left[\frac{L(k_0-k)}{N}\left(\frac{L(k_0+k)}{N}-2D_p^{fin}(\frac{n}{L})\right)\right]}. \tag{26}$$

If one denotes $\tilde{V}^g_{f_p}$ the estimation of $V^g_{f_p}$ given by (26), the retrieval of f_p can be carried out through:

$$f_p[n] \approx \frac{1}{g(0)N} \sum_{k=0}^{N-1} \tilde{V}^g_{f_p}[n,k]. \tag{27}$$

This technique applied to RRP-RD will be denoted by RRP-MR-LCR (LCR standing for *linear chirp reconstruction*).

To compare RRP-MR to reconstruction based on S-RD and MB-RD, it is natural to consider for each time n the interval:

$$\begin{aligned} \bar{I}_{LC}[n,\varphi_p[n]] &= \left[\lfloor \varphi_p[n] - 3std_{LC}[n,\varphi_p[n]\frac{N}{L}\rfloor, \lceil \varphi_p[n] + 3std_{LC}[n,\varphi_p[n]]\frac{N}{L}\rceil\right] \\ &:= [\overline{F}^-_p[n], \overline{F}^+_p[n]], \end{aligned} \tag{28}$$

which is the same as (24), except that D^{fin}_p is replaced by φ_p, and that the modulation is estimated by $\hat{q}_{\tilde{f}}[n,\varphi_p[n]]$ instead of $(D^{fin}_p)'$. Then the reconstruction of mode p is carried out by means of the formula:

$$f_p[n] \approx \frac{1}{g[0]N} \sum_{k\in[\overline{F}^-_p[n],\overline{F}^+_p[n]]} V^g_{\tilde{f}}[n,k]. \tag{29}$$

For the sake of a fair comparison with RRP-MR, if $[\overline{F}^-_p[n], \overline{F}^+_p[n]]$ intersects $[\overline{F}^-_{p+1}[n], \overline{F}^+_{p+1}[n]]$ these are replaced by $[\overline{F}^-_p[n], \frac{\overline{F}^+_p[n]+\overline{F}^-_{p+1}[n]}{2}]$ and $[\frac{\overline{F}^+_p[n]+\overline{F}^-_{p+1}[n]}{2}, \overline{F}^+_{p+1}[n]]$ respectively. This type of reconstruction technique used with S-RD or MB-RD are called S-MR and MB-MR respectively.

VI. Numerical Applications

In this section, we first investigate the quality of RRP-RD compared with S-RD and MB-RD on multicomponent simulated signals, in Section VI-A. Then, we assess the quality of the just described mode reconstruction techniques in Section VI-B, on the same simulated signals. We finally investigate the behavior of RRP-RD on a gravitational-wave signal in Section VI-C (all the Matlab programs enabling the figures reproduction is available at https://github.com/Nils-Laurent/RRP-RD). Note that to compute the STFT in all cases, we use a Gaussian window such that its standard deviation corresponds to the minimal Rényi entropy [25], which is proved to be a good trade-off minimizing interference between the modes in the TF plane [26]. We are aware of recent works on adaptive window determination as developed in [27], [28], but though to choose the window adaptively may ease ridge determination, adaptation require the knowledge of a rough version of the ridges, which is very critical in noisy situations.

A. Comparison on RRP-RD, S-RD and MB-RD on Simulated Signals

Our goal in this section is to show that RRP-RD is much more relevant in noisy situations than S-RD and MB-RD. For that purpose we compute RD results for the signals of Fig. 3, when the input SNR varies between -10 dB and 4 dB. We choose to consider only low input SNRs because at higher SNRs the modes are associated with a local maximum at each time instant, and the ridge detection is less challenging.

When the signal is made of two linear chirps as in Fig. 3 (a), the detection results depicted in Fig. 4 (a) tell us that RRP-RD performs much better than S-RD and MB-RD. Note that the approximation polynomials used in RRP-RD are both with degree 5 (to reduce their orders does not significantly change the results). For that example $L = 4096$ and Δt is set to 20, meaning the maximal time between two ridge portions associated with the same mode is $\frac{20}{4096}$ seconds and s defining the RRPs is set to 8. Comparing the results associated with S-RD and MB-RD, we notice that the former behaves better than the latter at low noise level and similarly at a higher noise level. Such a behavior is related to the fact that the modulation operator $\hat{q}_{\tilde{f}}$ is not accurate at locations where the ridge is split, and MB-RD fails to follow the different ridge portions corresponding to a mode (in these simulations, C is set to 2). On the contrary, since S-RD uses the fixed modulation parameter B_f (here set to 10), it is able to follow ridge portions that are not necessarily connected which explains why it works better that MB-RD at high noise level. On that example, for positive input SNRs, since S-RD and MB-RD lead to the same results, local maxima along the frequency axis of the spectrogram associated with each mode exist at each time instant: the gain in output SNR brought by RRP-RD arises from polynomial approximation. For negative input SNRs, such maxima no longer exist for each time instant and the gain brought by RRP-RD is related to the relevance of the grouping of RRPs.

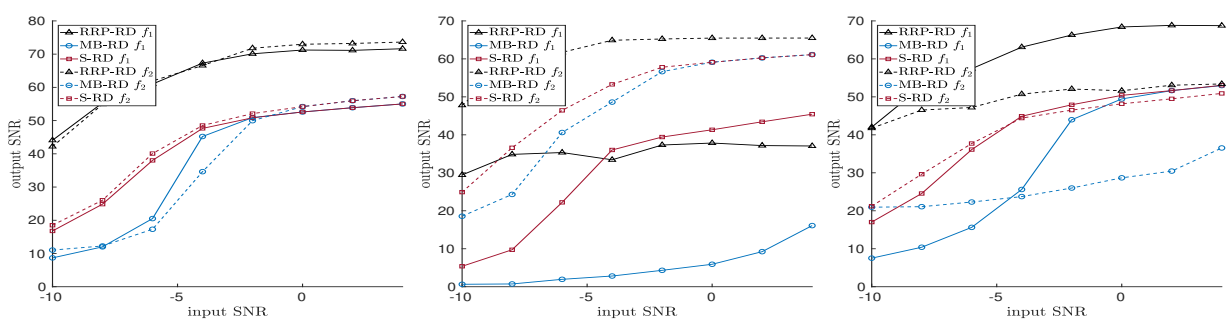

(a) (b) (c)

Fig. 4. (a): Comparison between S-RD, MB-RD and RRP-RD, for the signal of Fig. 3 (a): for each mode $p = 1, 2$, computation of output SNR between IF ϕ'_p and estimated IF with respect to input SNR (the results are averaged over 30 realizations of the noise); (b): same as (a) but for the signal of Fig. 3 (b); (c): same as (a) but for the signal of Fig. 3 (c)

Now, analyzing RD results for the signal of Fig. 3 (b), we remark that the conclusions for mode f_2 are similar to those for linear chirps. Indeed, at low input SNRs RRP-RD performs much better than the other two techniques since it better copes with the absence of a local maximum along the frequency axis close to the IF locations of the modes. On the contrary, when such maxima exist, namely for input SNRs such that S-RD and MB-RD coincide, the gain in terms of output SNR with RRP-RD is less important than in the case of linear chirps since to approximate a cosine phase with a polynomial of degree 5 leads to larger errors. As for mode f_1, which is much more modulated that f_2, we see that at a high noise level, RRP-RD is still much better than the other two techniques, but when the noise level decreases, S-RD behaves better than RRP-RD due to inaccuracy in IF approximation using a polynomial of degree 5. In such a case, since the modulation operator $\hat{q}_{\tilde{f}}$ is more sensitive to noise when the mode is more modulated, MB-RD behaves worse than the other two techniques.

Finally, regarding the signal of Fig. 3 (c), we only comment on the results related to the mode with exponential phase, for which we again notice that RRP-RD behaves much better than the other two tested methods at low input SNR, meaning the grouping of RRPs is still performing well in that case. When the noise level decreases, namely when f_2 generates a local maximum along the frequency axis at each time instant, RRP-RD and S-RD behaves similarly (an exponential phase can be accurately approximated by a polynomial with degree 5). On the contrary, the modulation operator $\hat{q}_{\tilde{f}}$ is not accurate enough to follow the local maxima along the frequency axis of the spectrogram of f_2.

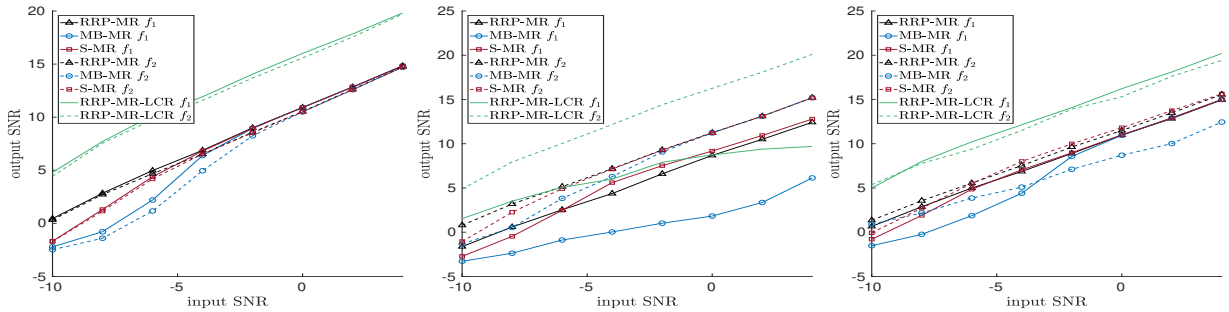

(a) (b) (c)

Fig. 5. (a): For each mode $p = 1, 2$, output SNR between mode f_p of signal of Fig. 3 (a) and reconstructed mode for each methods, namely S-MR, MB-MR, RRP-MR, and RRP-MR-LCR (the results are averaged over 30 noise realizations); (b): same but with signal of Fig. 3 (b); (c): same but with signal of Fig. 3 (c);

B. Comparison of the Mode Reconstruction Techniques

In this section, we investigate the quality of mode reconstrutcion techniques S-MR, MB-MR, RRP-MR, and RRP-MR-LCR still for the signals of Fig. 3. Looking at the results of Fig. 5 (a) related to the

signal of Fig. 3 (a), it transpires that while the RRP-RD is much better than S-RD and MB-RD at high noise levels this is not reflected in mode reconstruction. This is due to the fact that too much noise is included in intervals $[F_p^-[n], F_p^+[n]]$ and $[\overline{F}_p^-[n], \overline{F}_p^+[n]]$ for each n, and consequently the coefficients used for reconstrution are not relevant. Alternatively, when one considers RRP-MR-LCR, the results are significantly improved, meaning that at low SNR one had rather use the information on the ridge to reconstruct rather than summing the coefficients in the vicinity of the ridge. Such a conclusion remains true for the mode f_2 of the signal of Fig. 3 (b), and also for the mode f_1 of that signal, but only at low input SNRs. Indeed, at high input SNRs, RRP-MR-LCR is hampered by inaccuracy in phase approximation with a polynomial of degree 5, which entails larger errors in IF and CR estimations in the linear chirp approximation involved in this technique. Finally, for the signal of Fig. 3 (c), the reconstruction results are always much better with RRP-MR-LCR than with the other tested techniques (the ridge approximation provided by RRP-RD for the exponential chirp being of good quality). To conclude on that part, we should say that to reconstruct the modes in very noisy scenarios, one had rather use the information on the ridge to construct a linear chirp approximation than sum the coefficients in the TF plane.

C. Application to Gravitational-Wave Signals

In this section, we investigate the applicability of RRP-RD and RRP-MR-LCR to a transient gravitational-wave signal, generated by the coalescence of two stellar-mass black holes. This event, called **GW150914**, was detected by the LIGO detector Hanford, Washington and closely matches the waveform Albert Einstein predicted almost 100 years ago in his general relativity theory for the inspiral, the merger of a pair of black holes and the ringdown of the resulting single black hole [29]. The observed signal has a length of 3441 samples in $T = 0.21$ seconds.

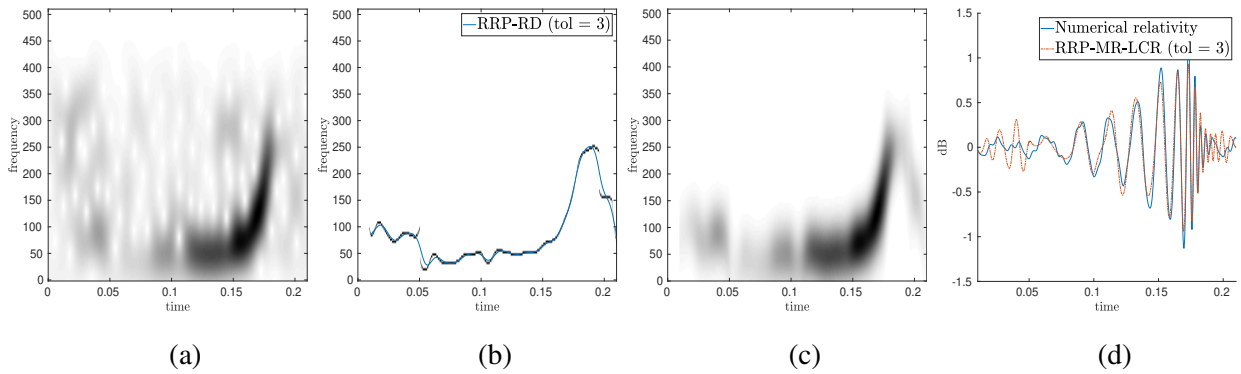

Fig. 6. (a): STFT of the Hanford signal; (b): Spline associated with RRP-RD (tol = 3) along with the ridge portion $\mathcal{M}^{fin}$; (c): Denoised STFT used by RRP-MR-LCR technique; (d): Signal reconstructed using RRP-MR-LCR along with the one predicted by numerical relativity.

We first display in Fig. 6 (a), the STFT of such a signal. Since the latter is first very slightly modulated during the inspiral phase, then behaves like an exponential chirp during the merging and as a fast decreasing phase during the ringdown, to try to approximate the instantaneous frequency with a polynomial in RRP-RD is not appropriate. Therefore, keeping the same formalism we use spline approximation instead. This means that, after the merging step, we consider the cubic spline s^0

$$s^0 = \underset{s \in S_{\mathcal{M}^0}}{\text{argmin}} \int_0^T (s''(t))^2 dt, \tag{30}$$

in which $S_{\mathcal{M}^0}$ is the spline space defined at the knots $\mathcal{M}^0$ (here we omit the subscript p because we look for a single mode), under the constraints:

$$\sum_{[n,k] \in \mathcal{M}^0} |k - s(\frac{n}{L})|^2 R(\mathcal{M}^0)^2 \leq D, \tag{31}$$

where D is a tolerance parameter that can easily related to a number of frequency bins: $tol = \frac{1}{R(\mathcal{M}^0)} \sqrt{\frac{D}{\#\mathcal{M}^0}}$, where $\#\mathcal{M}^0$ denotes the cardinal of $\mathcal{M}^0$, should be of the order of a few frequency bins. Then, the same type of approach as in the polynomial approximation is carried out, integrating new ridge portions in the minimization process, to obtain in the end the spline s^{fin} corresponding to the set of ridge portions $\mathcal{M}^{fin}$. The spline obtained using RRP-RD along with the set $\mathcal{M}^{fin}$ corresponding to the STFT of Fig. 6 (a) is displayed in Fig. 6 (b). Then, at each point on the spline, one can define a denoised STFT based on the linear chirp approximation following (26) in which D_p^{fin} is replaced by s^{fin}. Such a STFT is displayed in Fig. 6 (c). Finally, the signal reconstructed with RRP-MR-LCR is displayed in Fig. 6 (d) along with the signal given by the numerical relativity [30], showing a great similarity between the two signals. In this respect, to investigate the quality of mode reconstruction, we compute the SNR between the signals obtained with the different reconstruction techniques and that given by the numerical relativity. The results are displayed in Table I, showing that RRP-MR-LCR behaves slightly better than RRP-MR, and that each method is only slightly sensitive to the parameter tol.

tol	1	2	3
RRP-MR	7.6097	7.6403	7.6669
RRP-MR-LCR	8.4620	8.6645	8.7498

TABLE I

SNR BETWEEN THE SIGNALS OBTAINED WITH RRP-MR OR RRP-MCR-LR AND THE SIGNAL GIVEN BY THE NUMERICAL RELATIVITY

The results obtained here are interesting in that they reflect that RRP-RD enables the detection of the ringdown. Similar results were obtained using higher order syncrosqueezed STFT [31] or second order

synchrosqueezed continuous wavelet transform [32], but we here show that if one uses a robust ridge detector as RRP-RD, it is not necessary to reassign the transform to detect the ringdown.

VII. Conclusion

In this paper, we have introduced a novel technique to detect the ridges made by the modes of a multicomponent signal in the time-frequency plane. Our focus was to design the technique in such a way that it enables the computation of the ridges in very noisy situations. For that purpose we have brought about the notion of relevant ridge portions, which we subsequently used in our ridge detector. The proposed technique show significant improvements over state-of-the-art methods based on time-frequency representations on simulated signals, and is also interesting to analyze gravitational-wave signals. Some remaining limitations of the present work that it cannot deal with crossing modes and requires that the number of modes is fixed for the whole signal duration. In a near a future, we will investigate how to adapt our algorithm to such situations.

References

[1] R. Gribonval and E. Bacry, "Harmonic decomposition of audio signals with matching pursuit," *IEEE Transactions on Signal Processing*, vol. 51, no. 1, pp. 101–111, 2003.

[2] Y.-Y. Lin, H.-t. Wu, C.-A. Hsu, P.-C. Huang, Y.-H. Huang, and Y.-L. Lo, "Sleep apnea detection based on thoracic and abdominal movement signals of wearable piezoelectric bands," *IEEE journal of biomedical and health informatics*, vol. 21, no. 6, pp. 1533–1545, 2017.

[3] C. L. Herry, M. Frasch, A. J. Seely, and H.-T. Wu, "Heart beat classification from single-lead ecg using the synchrosqueezing transform," *Physiological Measurement*, vol. 38, no. 2, pp. 171–187, 2017.

[4] P. Flandrin, *Time-frequency/time-scale analysis*. Academic Press, 1998, vol. 10.

[5] B. Boashash, *Time frequency signal analysis and processing - A comprehensive reference*. Gulf Professional Publishing, 2003.

[6] L. Stankovic, M. Dakovic, and T. Thayaparan, *Time-frequency signal analysis with applications*. Artech house, 2014.

[7] F. Auger, P. Flandrin, Y.-T. Lin, S. McLaughlin, S. Meignen, T. Oberlin, and H.-T. Wu, "Time-frequency reassignment and synchrosqueezing: An overview," *IEEE Signal Processing Magazine*, vol. 30, no. 6, pp. 32–41, 2013.

[8] R. Carmona, W. Hwang, and B. Torresani, "Characterization of signals by the ridges of their wavelet transforms," *IEEE Transactions on Signal Processing*, vol. 45, no. 10, pp. 2586–2590, Oct 1997.

[9] ——, "Multiridge detection and time-frequency reconstruction," *IEEE Transactions on Signal Processing*, vol. 47, no. 2, pp. 480–492, Feb 1999.

[10] L. Stanković, "A measure of some time–frequency distributions concentration," *Signal Processing*, vol. 81, no. 3, pp. 621–631, 2001.

[11] L. Stankovic, M. Dakovic, and V. Ivanovic, "Performance of spectrogram as if estimator," *Electronics Letters*, vol. 37, no. 12, pp. 797–799, 2001.

[12] S. Meignen and D.-H. Pham, "Retrieval of the modes of multicomponent signals from downsampled short-time fourier transform," *IEEE Transactions on Signal Processing*, vol. 66, no. 23, pp. 6204–6215, 2018.

[13] M. A. Colominas, S. Meignen, and D.-H. Pham, “Fully adaptive ridge detection based on stft phase information,” *IEEE Signal Processing Letters*, 2020.

[14] I. Daubechies, J. Lu, and H.-T. Wu, “Synchrosqueezed wavelet transforms: an empirical mode decomposition-like tool,” *Applied and Computational Harmonic Analysis*, vol. 30, no. 2, pp. 243–261, 2011.

[15] G. Thakur, E. Brevdo, N. S. FučKar, and H.-T. Wu, “The synchrosqueezing algorithm for time-varying spectral analysis: Robustness properties and new paleoclimate applications,” *Signal Processing*, vol. 93, no. 5, pp. 1079–1094, May 2013.

[16] T. Oberlin, “Analyse de signaux multicomposantes : contributions à la décomposition modale empirique, aux représentations temps-fréquence et au synchrosqueezing,” Ph.D. dissertation, Mathématiques Appliquées de l’Université de Grenoble, Novembre 2013.

[17] R. Behera, S. Meignen, and T. Oberlin, “Theoretical analysis of the second-order synchrosqueezing transform,” *Applied and Computational Harmonic Analysis*, vol. 45, no. 2, pp. 379–404, 2018.

[18] C. Li and M. Liang, “A generalized synchrosqueezing transform for enhancing signal time–frequency representation,” *Signal Processing*, vol. 92, no. 9, p. 2264–2274, Sep 2012.

[19] S. Meignen, D.-H. Pham, and S. McLaughlin, “On demodulation, ridge detection, and synchrosqueezing for multicomponent signals,” *IEEE Transactions on Signal Processing*, vol. 65, no. 8, pp. 2093–2103, 2017.

[20] M. A. Colominas, S. Meignen, and D.-H. Pham, “Time-frequency filtering based on model fitting in the time-frequency plane,” *IEEE Signal Processing Letters*, vol. 26, no. 5, pp. 660–664, 2019.

[21] I. Djurović and L. Stanković, “An algorithm for the wigner distribution based instantaneous frequency estimation in a high noise environment,” *Signal Processing*, vol. 84, no. 3, pp. 631–643, 2004.

[22] X. Zhu, Z. Zhang, J. Gao, and W. Li, “Two robust approaches to multicomponent signal reconstruction from stft ridges,” *Mechanical Systems and Signal Processing*, vol. 115, pp. 720–735, 2019.

[23] S. Chen, Z. Peng, Y. Yang, X. Dong, and W. Zhang, “Intrinsic chirp component decomposition by using fourier series representation,” *Signal Processing*, vol. 137, pp. 319–327, 2017.

[24] N. Laurent and S. Meignen, “A novel time-frequency technique for mode retrieval based on linear chirp approximation,” *IEEE Signal Processing Letters*, 2020.

[25] R. G. Baraniuk, P. Flandrin, A. J. Janssen, and O. J. Michel, “Measuring time-frequency information content using the rényi entropies,” *IEEE Transactions on Information theory*, vol. 47, no. 4, pp. 1391–1409, 2001.

[26] S. Meignen, M. Colominas, and D.-H. Pham, “On the use of rényi entropy for optimal window size computation in the short-time fourier transform,” in *ICASSP 2020-2020 IEEE International Conference on Acoustics, Speech and Signal Processing (ICASSP)*. IEEE, 2020, pp. 5830–5834.

[27] L. Li, H. Cai, H. Han, Q. Jiang, and H. Ji, “Adaptive short-time fourier transform and synchrosqueezing transform for non-stationary signal separation,” *Signal Processing*, vol. 166, p. 107231, 2020.

[28] L. Li, H. Cai, and Q. Jiang, “Adaptive synchrosqueezing transform with a time-varying parameter for non-stationary signal separation,” *Applied and Computational Harmonic Analysis*, 2019.

[29] B. P. Abbott, R. Abbott, T. Abbott, M. Abernathy, F. Acernese, K. Ackley, C. Adams, T. Adams, P. Addesso, R. Adhikari *et al.*, “Observation of gravitational waves from a binary black hole merger,” *Physical review letters*, vol. 116, no. 6, p. 061102, 2016.

[30] B. P. Abbott, R. Abbott *et al.*, “GW151226: Observation of gravitational waves from a 22-solar-mass binary black hole coalescence,” *Physical Review Letters*, vol. 116, no. 24, p. 241103, 2016.

[31] D. H. Pham and S. Meignen, “High-order synchrosqueezing transform for multicomponent signals analysis-with an application to gravitational-wave signal.” *IEEE Trans. Signal Processing*, vol. 65, no. 12, pp. 3168–3178, 2017.

[32] S. Meignen, T. Oberlin, and D.-H. Pham, “Synchrosqueezing transforms: From low-to high-frequency modulations and perspectives,” *Comptes Rendus Physique*, vol. 20, no. 5, pp. 449–460, 2019.